LAWRENCE
LIVERMORE
NATIONAL
LABORATORY

LLNL-TR-608816

Recovering Large Volumes of Homogeneously Shocked Samples

S. T. Stewart

December 20, 2012

Disclaimer

This work performed under the auspices of the U.S. Department of Energy by Lawrence Livermore National Laboratory under Contract DE-AC52-07NA27344.

Final Report

NIF Concept Development Study

Title: Recovering Large Volumes of Homogeneously Shocked Samples

PI: Sarah T. Stewart, Harvard University

NNSA Award No. DE-AC52-07NA27344

1/30/2012 – 9/30/2012

Research Team

Richard Kraus, Harvard Graduate Student and Experiment Leader
Suzanne Ali, Berkeley Graduate Student
Laura Chen, Imperial Graduate Student
Tane Remington, UCSD Graduate Student
Damian Swift, LLNL
Cindy Bolme, LANL
Bruce Remington, LLNL
Brian Maddox, LLNL
Hye-Sook Park, LLNL

This work was supported by the following industry partners. General Atomics coined the rippled targets for shock recovery. Schaefer prepared the drive characterization targets for the pressure calibration.

At General Atomics:
Abbas Nikroo
Mike Farrell
Greg Randall
Reny Paguio
Paul Fitzsimmons

At Schaefer Laboratory:
Jon Streit
Nicole Petta
Thomas Bernat

Acknowledgements

We thank Gilbert Collins and Matt Cowan for their support of these concept development experiments. Brian Maddox, Damian Swift, Laura Chen generously donated time at Janus for the first test shots in June 2012. We also thank the JLF technical team and Bob Cauble for their support.

Attachments

Summary report on "Coined Ripples in mm-Thick Metal for Harvard's JANUS Strength-Recovery Experiments" from General Atomics.

Introduction

The physics of instability growth is crucial to understanding the chemistry and formation of the Earth. The final phase of Earth's formation was dominated by giant impact events between Mars-size bodies, called planetary embryos. Each embryo grows separately from the others, recording a chemical fingerprint of its unique accretion history. In low-resolution hydrocode simulations of an embryo colliding with the proto-Earth (e.g., the moon-forming impact), the iron cores of the two bodies rapidly merge, without mechanical mixing. However, geochemical data suggests the core and mantle of the growing Earth achieved some chemical equilibration. Rayleigh-Taylor instabilities (RTI), which are unresolved in the hydrocode simulations, are expected to be the dominant mechanism for breakup of the impactor's iron core while sinking through the Earth's mantle . However, prior to Rayleigh-Taylor growth, the shock wave propagating through the impactor's mantle and core is unstable to Richtmyer-Meshkov instabilities (RMI), which could seed the growth of RTI.

The growth of instabilities is also detrimental to an inertial confinement fusion capsule as it can poison the fusion reaction. Consequently, understanding instability growth at accelerated and shocked interfaces is an active research area and a central component of the research program at the National Ignition Facility (NIF).

Summary of NIF Concept Development Goals and Results

We proposed the development of a laser platform recovery system for large samples. We designed and tested a recovery system for targets subject to RMI and/or RTI growth. The recovery experiments, performed at the Janus laser in the Jupiter Laser Facility (JLF) in June and August 2012, were successful.

The recovered samples of Ta and Fe are being used (i) to improve the physical understanding and scaling of instability growth in materials with strength and (ii) to investigate the microstructural evolution during the stages of instability growth. Comparison of measurements of instability growth in situ and in recovered samples will be used to assess the fidelity (interpretability) of the quenched dynamic processes recorded in the recovered samples. Well-characterized recovery experiments are desired in order to allow for detailed chemical and microstructural analyses. Based on these results, science team member Bruce Remington will propose to conduct recovery experiments at the Omega laser to reach higher shock pressures and larger amplitudes of instability growth.

Background

The uncorrupted recovery of targets shocked using a plate impact system is difficult. Due to the large momentum associated with the flyer plate and sabot, complicated recovery assemblages must be used to decelerate not only the target, but the flyer plate and sabot as well [*Bourne and Gray III*, 2005a; b]. For plate impact velocities above 1 km/s, it is almost impossible to perform recovery on samples that have not been modified by strong secondary tensile and compressive waves [*Gray III*, 2009]. Consequently, for recovery of strongly shocked samples, it is necessary to employ a different driving

mechanism. As a disclaimer, it would be incorrect to say that samples have not been recovered from higher pressure experiments, thin films have been recovered in gas gun experiments up to 1 Mbar [e.g., *Nellis and Gratz*, 1993]. However, such samples are loaded with a complicated pressure and thermal history due to the required recovery system, a pressure history that is not generally seen during planetary impact events.

Owing to the lack of a sabot, explosively and magnetically launched flyer plates require a smaller amount of momentum to be decelerated by the recovery assembly. However, expanding detonation products or shot hardware and a thick flyer still provide a large amount of additional momentum to the target.

Recovery of a target subject to shock waves induced via x-ray ablation from a Z-pinch experiment at Sandia National Laboratory have recently been attempted [*Remo and Furnish*, 2008]. However, shot hardware penetrated their recovery fixture and destroyed the sample. Remo and Furnish [2008] also noted that the intense x-ray flux likely deteriorated their samples on the microscopic level as well.

Due to the practically momentum-free drive, laser-driven shock waves offer an unmatched opportunity for the recovery of targets with known, and tunable, loading histories. A number of experiments have been performed on the recovery of small targets from laser driven shock wave experiments [*Luo et al.*, 2005; *Luo et al.*, 2004; *Meyers et al.*, 2003]. Utilizing large backing windows to absorb the momentum, metallic samples are easily recovered [*Luo et al.*, 2004]. Researchers have also used lasers as point sources of energy to simulate the stress field around an impact crater [*Petaev et al.*, 2008; *Remo et al.*, in preparation]; however, the loading history in the samples was not well known.

Recovered samples that have undergone RMI or RTI growth are needed to determine the microscopic processes controlling the flow stress in a growing instability. To our knowledge, only two recovery experiments have been performed that suggest observation of RMI growth and no recovery experiments have been performed on RTI growth at high strain rates. Jacobsen et al. [2009] described chemical analyses of direct laser ablation experiments of an iron-olivine powder mixture at the Sandia Z-beamlet. Within the shocked material at the base of the crater, they find enhanced chemical mixing that they suggest could not be explained by diffusion alone. To explain the length scale of mixing they conclude that R-M instabilities increased the length scale of mixing during the experiment, which they hope to extrapolate to the mixing of iron cores during giant planetary impacts. Tschauner et al. [2005] performed a gas-gun shock recovery experiment of a mantle silicate and found droplets of the steel recovery cell embedded in the recovered target. They found the droplet size distribution to be consistent with what would be created by R-M instabilities at a rough interface.

Neither of these previous recovery experiments could be used to quantitatively understand the process of R-M or R-T instability growth in materials with strength; the experiments were too complicated to quantitatively analyze. For example, in these experimental configurations, it is not clear whether the instability growth occurred upon loading or decompression from the shocked state.

Laser experiments are often limited by sample size due to the generally low energy of the drive. However, NIF samples may be as large as gas gun samples or greater depending on the desired pressure. Consequently material questions with inherent length

scales greater than those achievable on smaller laser systems are accessible problems at NIF. However, given the shot rate and experimental cost, NIF is not the facility to optimize target recovery designs. The Jupiter Laser Facility serves a vital role for high-energy science, as the platform provides the ability to perform high quality science (over the available range) and the opportunity for low-cost testing and optimization of designs for dynamic recovery systems on higher energy platforms.

The development of an ultra-high pressure recovery system was noted as one of the research needs at a recent NIF Science Workshop [*Sarrao et al.*, 2011]. The experiments performed here are in direct support of that goal. In this report, we discuss the result of our NIF concept development study to develop a recovery system and to recover samples of Ta and Fe that have undergone RMI growth.

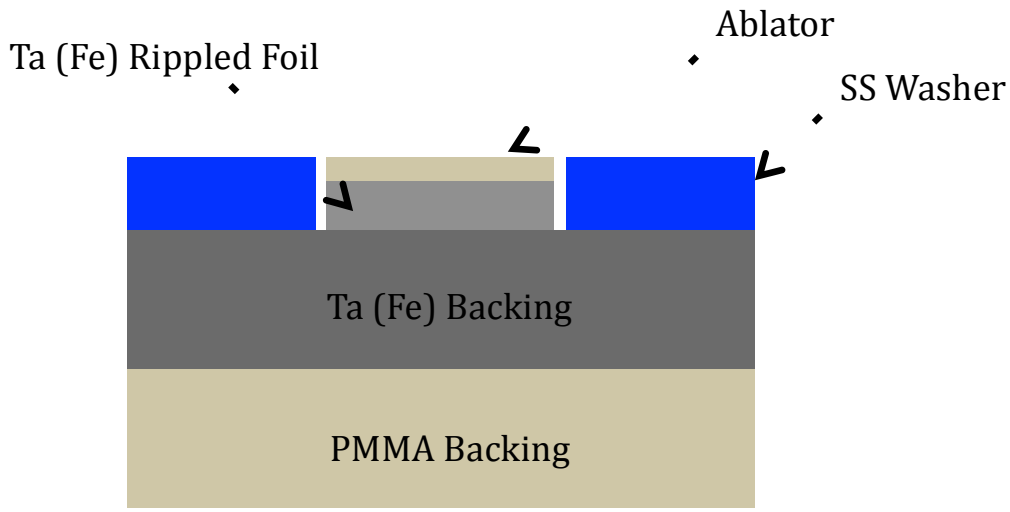

Figure 1: Schematic design for high-pressure recovery of rippled Ta and Fe foils. The ablator package was made of 244(5) micron polystyrene (CH). The drive surface was coated with 130 nm of Al to prevent any pre-pulse from degrading the rippled interface. In some cases, the ablator also included an approximately 50-micron thick Br-doped CH ablator to prevent high energy x-rays from melting the Ta (Fe) interface. The Ta (Fe) foil is then clamped into a larger recovery fixture so the foil to prevent separation of the target from the thicker backing plate upon decompression.

Methods

The Janus laser at the Jupiter laser facility is a two-beam Nd:glass laser capable of delivering up to ~350 J per beam at the frequency doubled wavelength of 527 nm for pulse lengths of 2 to 10 ns. The laser beams were focused onto the target and a random phase plate was used to create a square spot with an area of ~1.4 mm^2. Due to the variability in the pulse shaping at the Janus laser, a pulse duration of 4 ns and a thick ablator was used, which caused the shock wave created at the ablation surface to decay into a Taylor wave upon interaction with the sample.

A schematic of the recovery target is presented in Figure 1. The samples of Ta and Fe were coined using a nitrided steel die and 15 ton press at General Atomics to create the seed instability perturbation. An amplitude of 10 microns and a wavelength of 50 microns was used to be within the expected range of linear instability growth but also of sufficient amplitude to ensure a measureable change in amplitude in recovered targets. This seed perturbation is of greater amplitude than has previously been coined at GA and represents significant development in their coining process.

In gas gun shock recovery targets, multiple lateral and downrange momentum traps are often used; however, the scale of laser targets are sufficiently small so that the targets themselves can be of sufficient size for the shock wave to decay to nearly, or below the elastic limit upon the drive wave reaching the downrange free surface. Any reflected waves will then be of sufficiently small amplitude to significantly reduce the chance of spall or fracture within the sample. For the targets shown in Figure 1, the Ta (Fe) rippled sample is 1-mm thick, the Ta (Fe) backing plate was 4-mm thick, and a 3-mm thick PMMA window was used to further damp the release wave at the downrange free surface. The Ta (Fe) rippled samples were 3 mm in diameter and the backing plates and windows were 10 mm in diameter. In this development study, we also considered the use of a high-impedance mixture of tungsten and epoxy that could be used as a lateral impedance matching material that would be well suited for future experiments on samples of lower or similar impedance to Fe. Our initial test shots indicated that such a lateral momentum trap was not needed for the pressures achieved at Janus and the tungsten-epoxy mixture was not used.

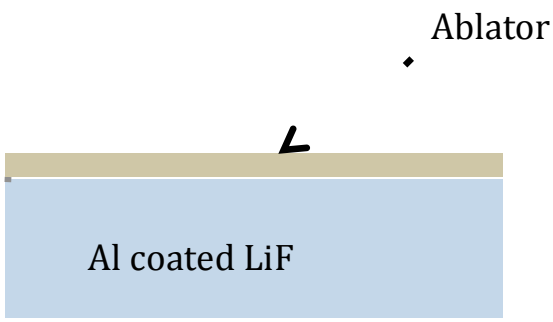

Figure 2: Schematic of a drive characterization target for pressure calibration in recovered targets. The ablator package is the same as shown in Figure 1. The LiF window was coated with 7.5 microns of Al so the reflecting interface between the Al and LiF would act as a Lagrangian particle velocity gauge with the VISAR diagnostic. The free surface of the LIF window was AR coated to minimize secondary reflections within the VISAR diagnostic.

The thickness of the recovery target assembly precludes the ability to measure the shock state in-situ with a velocimetry diagnostic such as VISAR. Therefore, to characterize the drive in the sample, we performed a separate suite of experiments with

the same ablator package backed by a LiF window coated with 7.5 microns of aluminum. A schematic of the LiF drive characterization targets, made by Schaefer Laboratory under their JLF support contract, is shown in Figure 2. For the range of drive energies considered in the recovery experiments, we measured the particle velocity at the LiF/ablator interface. The scaling of peak particle velocity at the LiF interface as a function of drive energy is shown in Figure 3a. As the equation of state of LiF, Ta, and Fe are well known, we used the impedance matching technique to determine the shock states at the Ta and Fe interfaces as a function of drive energy, Figure 3b.

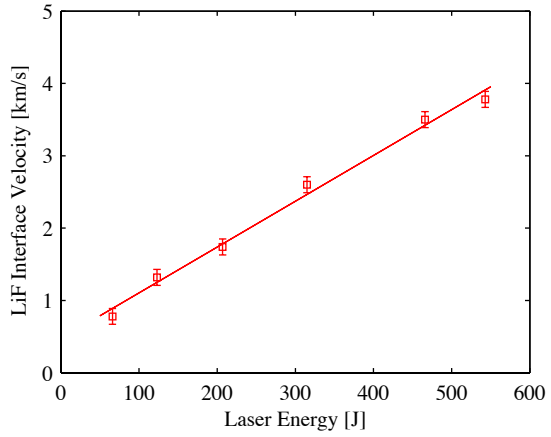

Figure 3a: Particle velocity at the Al-coated LiF interface (see Figure 2) as a function of drive laser energy. The drive laser pulse was 4 ns in duration and approximately square in shape.

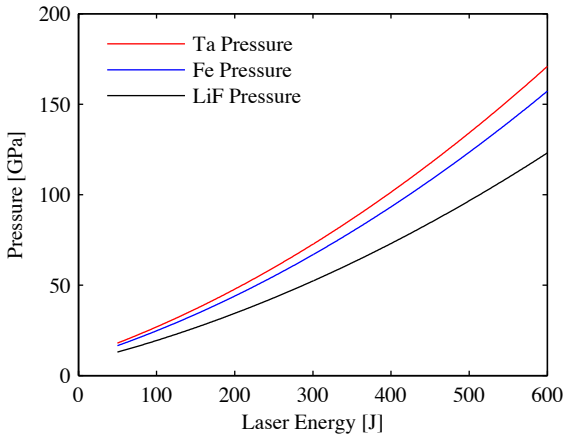

Figure 3b: Peak shock pressures as a function of drive laser energy. The stresses in Ta and Fe were determined using the scaling law shown in Figure 3a and the known relative shock-up states from LiF to Ta and LiF to Fe, respectively.

Although the laser intensity was relatively low, ~10^{12} W/cm^2, for a subset of the targets, a 30-micron layer of 12.5 atom percent Br-doped polystyrene was used to attenuate any high energy x-rays produced at the ablation surface. This layer was added to ensure that pre-heat from the x-rays did not modify the Ta (Fe) interface prior to interaction with the shock. Separate drive characterization experiments were performed with the Br-doped CH layer.

Observations

During the allotted time at the Jupiter laser facility, we performed a total of 20 shock recovery experiments on rippled Ta and Fe targets with input stresses ranging from approximately 20 to 150 GPa. All of the samples were recovered within the fixture and are intact.

Images of the rippled surfaces of Ta samples shocked to pressures ranging from 39 to 147 GPa as shown in Figures 4 to 6. Images of the rippled surfaces of Fe samples

shocked to pressures of 43 and 76 GPa are shown in Figures 7 and 8. Also shown in each figure are lineouts from surface profiles taken across the center of the drive spot on the recovered rippled interfaces.

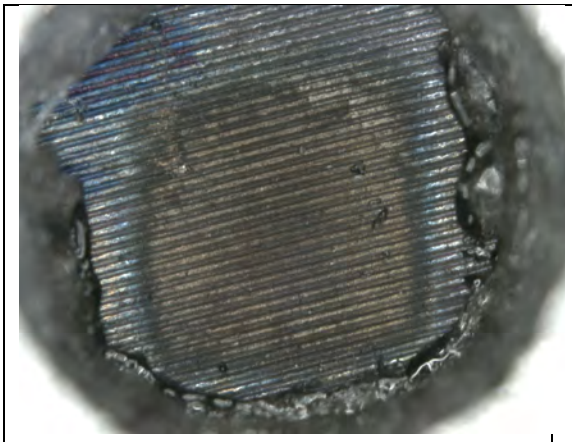

Figure 4a: Tantalum sample A2-1, 160 J, 39 GPa. The square discoloration correlates with the square phase plate. The size of the image is approximately 2.5 mm across with a ripple wavelength of 50 microns.

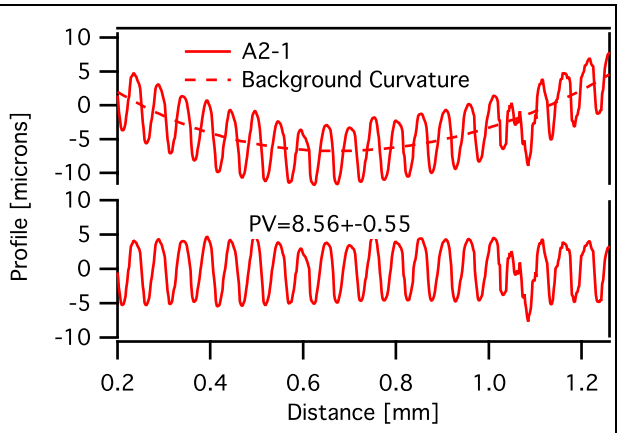

Figure 4b: Lineout from surface profile of recovered Ta sample shown in Figure 4a. The lineout was taken across the center of the drive spot. The top axis is the raw lineout and the bottom axis shows the surface profile with the background curvature subtracted. The peak-to-valley (PV) distance was obtained by averaging over 6 ripples in the center of the crater, where the uncertainty is the standard deviation of the PV distance of individual peaks. The pre-shot PV distance was 9.9(1.6) microns.

Figure 5a: Tantalum sample A2-2, 275 J, 66 GPa. The square discoloration correlates with the square phase plate. The source of the interior discoloration is not clear. The size of the image is approximately 2.5 mm across with a ripple wavelength of 50 microns.

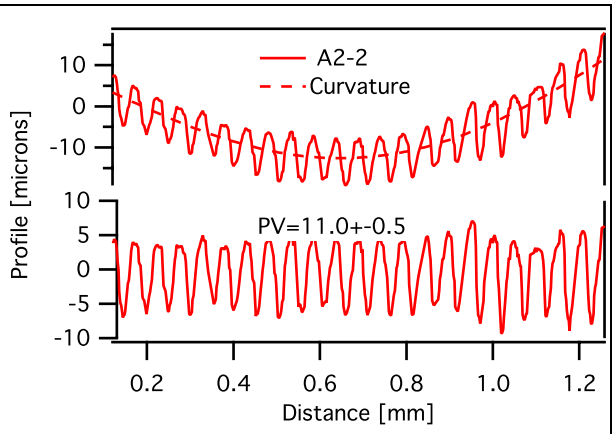

Figure 5b: Lineout from surface profile of recovered Ta sample shown in Figure 5a. The lineout was taken across the center of the drive spot. The top axis is the raw lineout and the bottom axis shows the surface profile with the background curvature subtracted. The peak-to-valley (PV) distance was obtained by averaging over 6 ripples in the center of the crater, where the uncertainty is the standard deviation of the PV distance of individual peaks. Note that the top axis and bottom axis ranges are not the same. The pre-shot PV distance was 9.6(1.8) microns.

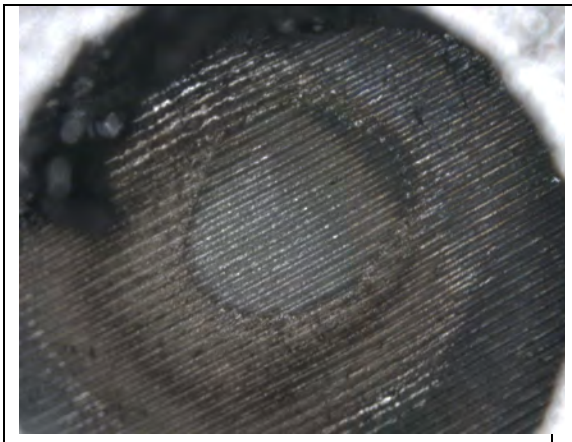

Figure 6a: Tantalum sample A2-3, 537 J, 147 GPa. The square discoloration correlates with the square phase plate. The source of the interior discoloration is not clear. The size of the image is approximately 2.5 mm across with a ripple wavelength of 50 microns.

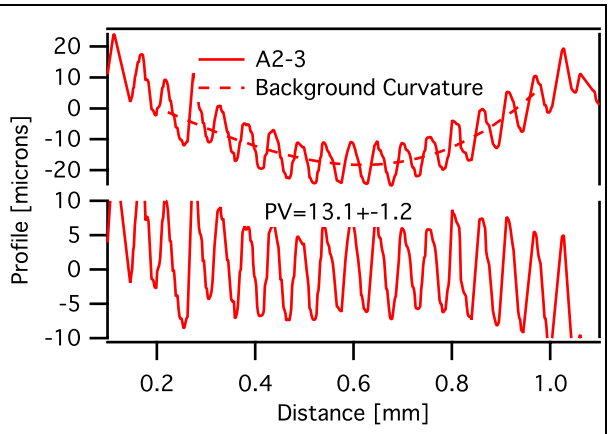

Figure 6b: Lineout from surface profile of recovered Ta sample shown in Figure 6a. The lineout was taken across the center of the drive spot. The top axis is the raw lineout and the bottom axis shows the surface profile with the background curvature subtracted. The peak-to-valley (PV) distance was obtained by averaging over 6 ripples in the center of the crater, where the uncertainty is the standard deviation of the PV distance of individual peaks. Note that the top axis and bottom axis ranges are not the same. The pre-shot PV distance was 10.7(1.5) microns.

Figure 7a: Iron sample B2-1, 198 J, 43 GPa. The square discoloration correlates with the square phase plate. The size of the image is approximately 2.5 mm across with a ripple wavelength of 50 microns.

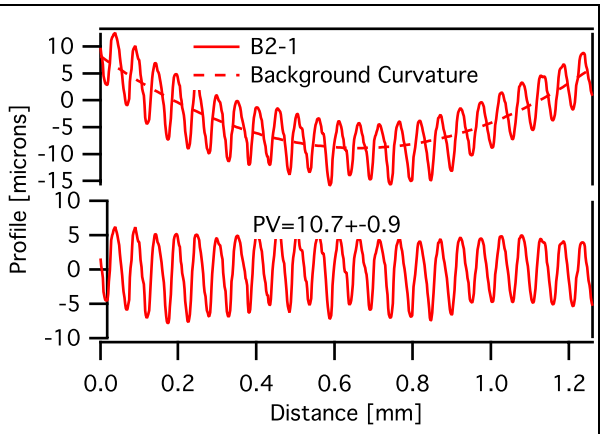

Figure 7b: Lineout from surface profile of recovered Fe sample shown in Figure 7a. The lineout was taken across the center of the drive spot. The top axis is the raw lineout and the bottom axis shows the surface profile with the background curvature subtracted. The peak-to-valley (PV) distance was obtained by averaging over 6 ripples in the center of the crater, where the uncertainty is the standard deviation of the PV distance of individual peaks. Note that the top axis and bottom axis ranges are not the same. The pre-shot PV distance was 10.3(9) microns.

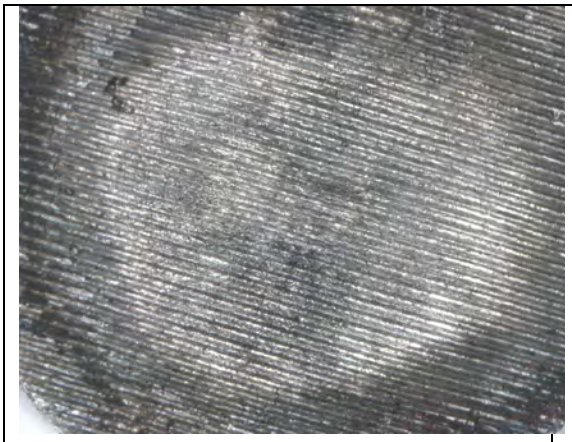

Figure 8a: Iron sample F2-2, 337 J, 76 GPa. The square discoloration correlates with the square phase plate. The size of the image is approximately 2.5 mm across with a ripple wavelength of 50 microns.

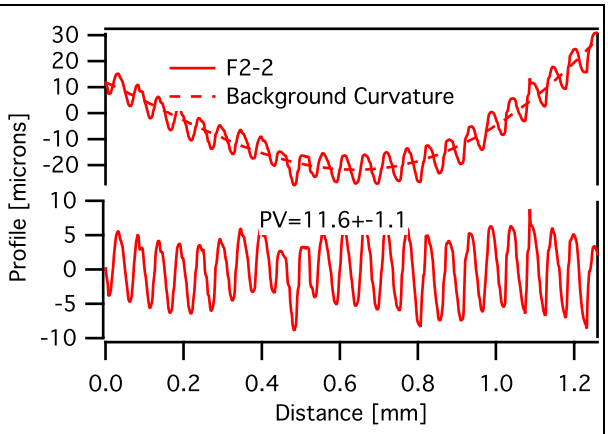

Figure 8b: Lineout from surface profile of recovered Fe sample shown in Figure 8a. The lineout was taken across the center of the drive spot. The top axis is the raw lineout and the bottom axis shows the surface profile with the background curvature subtracted. The peak-to-valley (PV) distance was obtained by averaging over 6 ripples in the center of the crater, where the uncertainty is the standard deviation of the PV distance of individual peaks. Note that the top axis and bottom axis ranges are not the same. The pre-shot PV distance was 8.3(3.6) microns.

Conclusions

Rippled samples of Ta and Fe were successfully recovered from shock states ranging from 20 to 150 GPa. RMI growth was observed in both the Ta and Fe samples. The simple recovery system used in these series of experiments proved effective. Future modifications will include using larger diameter coined samples and testing the W-epoxy lateral impedance matching fluid.

These results indicate that future shock recovery experiments on higher energy laser platforms such as Omega and NIF are likely to be successful.

Dissemination of Results

As the experiments were performed during the final month of the funding cycle, all of the data has not been completely analyzed. Future analyses will include detailed surface profilometry on all the recovered samples and microstructural characterization on a number of the Ta and Fe foils to determine how the large plastic flow modified the crystal structure. We plan to present these results at the 2013 Joint SCCM/AIRPT meeting and to publish our experimental results in a journal such as the *International*

Journal of Impact Engineering. We also plan to perform detailed model/experiment comparisons to determine the viability of Ta and Fe strength models for use in hydrocodes where large plastic strains occur.

References

Bourne, N. K., and G. T. Gray III (2005a), Computational design of recovery experiments for ductile metals, *Proceedings of the Royal Society A-Mathematical Physical and Engineering Sciences*, *461*(2062), 3297-3312.

Bourne, N. K., and G. T. Gray III (2005b), Soft-recovery of shocked polymers and composites, *Journal of Physics D: Applied Physics*, *38*(19), 3690.

Gray III, G. T. (2009), personal communication.

Jacobsen, S. B., J. L. Remo, M. I. Petaev, and D. D. Sasselov (2009), Hf-W Chronometry and the Timing of the Giant Moon-forming Impact on Earth, *Lunar Planet. Sci. Conf.*, Abstract #2054.

Luo, S.-N., O. Tschauner, T. E. Tierney, I. V. D. C. Swift, S. J. Chipera, and P. D. Asimow (2005), Novel crystalline carbon-cage structure synthesized from laser-driven shock wave loading of graphite, *The Journal of Chemical Physics*, *123*(2), 024703-024705.

Luo, S. N., D. C. Swift, T. E. Tierney, D. L. Paisley, G. A. Kyrala, R. P. Johnson, A. A. Hauer, O. Tschauner, and P. D. Asimow (2004), Laser-induced shock waves in condensed matter: some techniques and applications, *High Pressure Research*, *24*(4), 409-422.

Meyers, M. A., F. Gregori, B. K. Kad, M. S. Schneider, D. H. Kalantar, B. A. Remington, G. Ravichandran, T. Boehly, and J. S. Wark (2003), Laser-induced shock compression of monocrystalline copper: characterization and analysis, *Acta Materialia*, *51*(5), 1211-1228.

Nellis, W. J., and A. J. Gratz (1993), Recovery of materials impacted at high velocity, *Int. J. Impact Eng.*, *14*(1–4), 531-539.

Petaev, M. I., S. B. Jacobsen, R. G. Adams, and D. D. Sasselov (2008), Experimental Study of High-Energy Processing of Protoplanetary Materials: Implications for the Post-Giant-Impact Earth, *Lunar Planet. Sci. Conf.*, Abstract #1850.

Remo, J. L., and M. D. Furnish (2008), Analysis of Z-pinch shock wave experiments on meteorite and planetary materials, *Int. J. Impact Eng.*, *35*(12), 1516-1521.

Remo, J. L., S. B. Jacobsen, M. I. Petaev, R. G. Adams, and D. D. Sasselov (in preparation), Laser-shock melting of a metal-silicate target and the timing of the giant Moon-forming impact on Earth, *Nature*.

Sarrao, J., K. Budil, and M. Wiescher (Eds.) (2011), *Basic Research Directions for User Science at the National Ignition Facility*, Report on the National Nuclear Security Administration (NNSA) – Office of Science (SC) Workshop on Basic Research Directions on User Science at the National Ignition Facility, May 9-12, 2011, Washington D.C.

Tschauner, O., M. J. Willis, P. D. Asimow, and T. J. Ahrens (2005), Effective liquid metal-silicate mixing upon shock by power-law droplet size scaling in Richtmyer-Meshkov like perturbations, *Lunar Planet. Sci. Conf.*, Abstract #1802.

Coined Ripples in mm-Thick Metal for Harvard's JANUS Strength-Recovery Experiments

September 12, 2012

Michael Farrell	Greg Randall	Reny Paguio	Paul Fitzsimmons
farrell@fusion.gat.com	randall@fusion.gat.com	paguior@fusion.gat.com	fitzsimmons@fusion.gat.com
858-455-3975	858-455-3954	858-455-3953	858-455-2052
MS: G09-339A	MS: G22T- 104	MS: G09-351C	MS: G09-025

General Atomics, Inertial Fusion Technologies, 3550 General Atomics Ct., San Diego, CA 92121

I. SUMMARY

This memo summarizes 1 mm thick rippled tantalum (Ta) and iron (Fe) targets for Harvard's Strength-Recovery experiments on the JANUS laser. Because these materials are not diamond turnable, we used a coining process (developed previously) to pattern ripples in thin ~ 50 μm Ta and Fe foils [1]. The requested rippled pattern was a peak-to-valley (PV) ~ 10 μm and a wavelength (λ) = 50 μm, and each sample was ~3 mm diameter disc shape. These JANUS targets were our first coining attempts on metal foils ≥ 85 μm thick and the first with PV depths over 7 μm. This project required ~20 targets in a short lead time, so an increased the coining area, enabling two targets to be cut from one disc. Additionally, multiple coining runs were performed per each nitrided steel coining die.

We found the following:

1) the JANUS ripple pattern can be diamond turned with marginal clearance issues
2) a PV = 10 μm was successfully coined for the first time
3) a tool steel die will gradually depress in the center after multiple uses
4) the required coining stress is significantly lower for 1 mm thick discs than for thin foils, and
5) a 1 mm thick disc compresses ~ 10-15% during coining, Ta more so than Fe.

II. EXPERIMENTAL & DISCUSSION

A. Metal disc raw materials

The tantalum discs were 3N5 purity from ESPI Metals (Ashland, Oregon, Knd3317), annealed then as-rolled. The iron discs were 3N5 purity from ESPI Metals (Knd3316), likely annealed then as-rolled. Both were received as 6 mm diameter discs, 1.2 mm thick. Tantalum is resistant to oxidation at processing conditions used, however, iron can oxidize in room air or in water. Previous Auger tests on similarly processed iron foils showed an oxidation layer of < 20 nm thick [1].

B. Polishing

Each disc was polished on the intended rippled face down to a thickness of ~ 990 ± 10 μm using an Allied High Tech MultiPrep System and a polishing procedure similar to that in Randall et al. [1], progressing gradually from 600 SiC paper to colloidal silica for Ta and 600 SiC to 3 μm diamond for Fe to obtain low-worked surfaces. Roughness was determined by interferometry (Wyko NT9100, Veeco).

C. Coining procedure

Five 6.3 mm diameter, nitrided H13 steel dies were diamond turned for this delivery. The coining stress was applied by a 4-post 15-ton hydraulic press (3893.4NE1, Carver) with two plates that could be independently heated (200°C for both used here). We balanced a polished tool steel flat (Rockwell Hardness C63 testing block, Wilson Hardness, Norwood, MA, 9203191) on top of the disc/die/holder, and care was taken to avoid orientations where the disc would slip in the press. We coined each sample for 10 min at 200°C using 2000-8000 lb loads. The process is shown in Fig. 1(a).

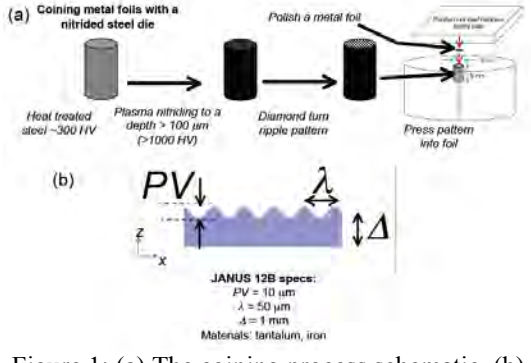

Figure 1: (a) The coining process schematic. (b) Parameter definitions: PV =peak-to-valley distance, λ=wavelength, Δ=disc thickness

D. Ripple characterization

The main parameters of the rippled disc are listed in Fig. 1(b). We sought to characterize the disc thickness (Δ) and peak-

to-valley distance of the ripple (PV). We used the Wyko NT9100 interferometer with Vision software to obtain the rippled disc surface profile at 50× (0.55× secondary) magnification, VSI setting, 1× speed, 1% threshold, and full precision. The high numerical aperture of the 50× objective was required to observe the reflected light in these deep, steep-walled patterns. The Wyko scans were stitched with automated software over a lineout across the center of each part, perpendicular to the ripple wavefronts. For analysis, we used the "Remove Tilt Only" Analysis Option, which subtracts out tilt from a slightly tilted stage. We also applied a Fourier analysis to determine the quality of the sine wave that we coined. This was done using the power spectral density (PSD) analysis of our interferometry scan. We reported the PSD ratio of the intended sine harmonic (positioned at the inverse wavelength) versus the secondary harmonic (positioned at two times the inverse wavelength). Quality sine wave pattern transfer will show PSD ratios greater than 10. The thickness of each disc was determined by a lineout reading on a dual confocal microscope, which consists of two Keyence LT9010M position sensors placed on either side of the disc suspended over a gap.

Using the Wyko lineout, we employed a custom automated program to extract the detailed peak-to-valley (PV) distribution. This called for smoothing derivative data of the stitched Wyko scan, determining the coordinates of peaks and valleys and averaging PV measurements over a nearest neighbor to account for the bowing slope in each part. Each data point corresponds to a peak-valley-peak trio (or valley-peak-valley) so n wavelengths generate $2n - 1$ PV points. Similar characterization work was done on some of the diamond turned dies.

We note that ripple quality was more variable than in previous work with thin foils. Figure 2 gives characteristic profiles for three separate quality classifications ("A", "B", and "C") and gives descriptions of each. It is currently unknown why the quality was variable since some discs coined at the exact same conditions varied from "A" to "C". Die deformation is a possible source. Another possible explanation stems from the large degree of compression the disc experiences during coining. Further work is necessary to understand this variability.

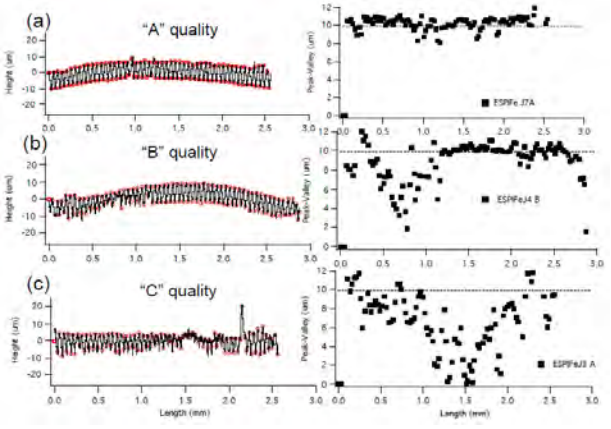

Figure 2: Coining quality characterization. "A" typically had high ripple uniformity over the disc surface with PV from 9.4-10.7 μm. "B" had uniformity issues and/or PV from 7.9-9.4 μm. "C" had large regions of poor transfer and PV < 8.3 μm.

E. Laser cutting multiple targets from the thick metal disc

To double productivity, we laser cut two targets out of one 6 mm coined disc (Fig. 3). The resulting targets were 2.9 mm in diameter. Note that due to the non-uniform compression, we expected some of the individual laser cut pieces to have a slight wedge profile with at most ~10 μm/mm slope. However, this is not true in all cases and is more of a worse-case, as the wedge profile depends on degree of compression as well as laser cutting positioning. Note that if the target diameter was slightly reduced, more of the coined material could be used (three parts per 6 mm coined foil).

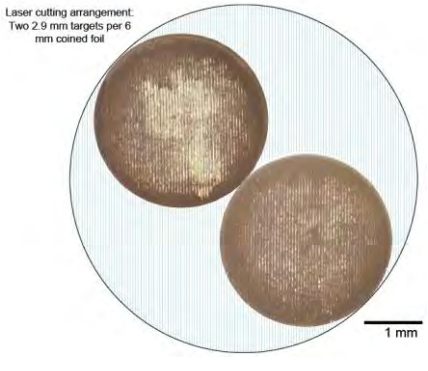

Figure 3: Geometry where two 2.9 mm targets are laser cut form a single coined 6 mm disc.

F. Tabulated results for individual targets

The post-coined, post-laser cut characterization results for each JANUS 12B target are tabulated in Table 1 for tantalum and Table 2 for iron. Figures 4a and 4b show examples of characterization results of "A" quality Ta and Fe targets. Importantly, note that this is the first coining batch of PV = 10 μm ripples. The previous maximum was 7 μm in our thin foil work. However, it is likely that the large thickness made it easier to coin these deep ripples, since the effective strain (PV/Δ) was still small (~ 1 %) here.

Multiple data and image files were uploaded to Harvard's ftp site (ftp://ft.rc.fas.harvard.edu/). A list of these files is

provided at the end of this memo.

	$\langle\Delta\rangle$	Coining weight, previous die runs	$\langle PV\rangle$	PSD ratio	Quality
Material	[μm]	[lbs]	[μm]	[μm]	
Ta3A	959	3500, 1	8.9	75	B
Ta4A	929	4000, 2	9.7	40	A
Ta4B	938	4000, 2	9.4	58	A
Ta5A	911	4300, 0	9.5	103	A
Ta5B	904	4300, 0	10.2	97	A
Ta6A	894	4100, 1	9.9	37	A
Ta6B	904	4100, 1	9.6	38	A
Ta7A	849	4300, 2	10.7	36	A
Ta7B	839	4300, 2	10.0	19	A
Ta8A	834	4300, 3	9.9	33	A
Ta8B	835	4300, 3	9.8	30	A
Ta12A	887	4300, 2	7.6	35	C
Ta12B	882	4300, 2	8.3	na	C

Table 1: Tantalum target thickness (Δ) and coining results (6 mm die, 200°C). PV of the dies ranged from 10.5-11.0 µm. Pre-coin thicknesses ranged from 980-1000 µm.

	$\langle\Delta\rangle$	Coining weight, previous die runs	$\langle PV\rangle$	PSD ratio	Quality
Material	[μm]	[lbs]	[μm]	[μm]	
Fe2A	934	6000, 3	7.9	17	B
Fe2B	920	6000, 3	9.7	33	A
Fe3A	927	6700, 5	7.2	33	C
Fe3B	933	6700, 5	8.3	29	C
Fe4A	923	6700, 0	9.0	93	B
Fe4B	907	6700, 0	10.0	46	A
Fe7A	908	6500, 6	10.3	58	A
Fe7B	895	6500, 6	9.6	53	A

Table 2: Iron target thickness (Δ) and coining results (6 mm die, 200°C). PV of the dies ranged from 10.5-11.0 µm. Pre-coin thicknesses ranged from 980-1000 µm.

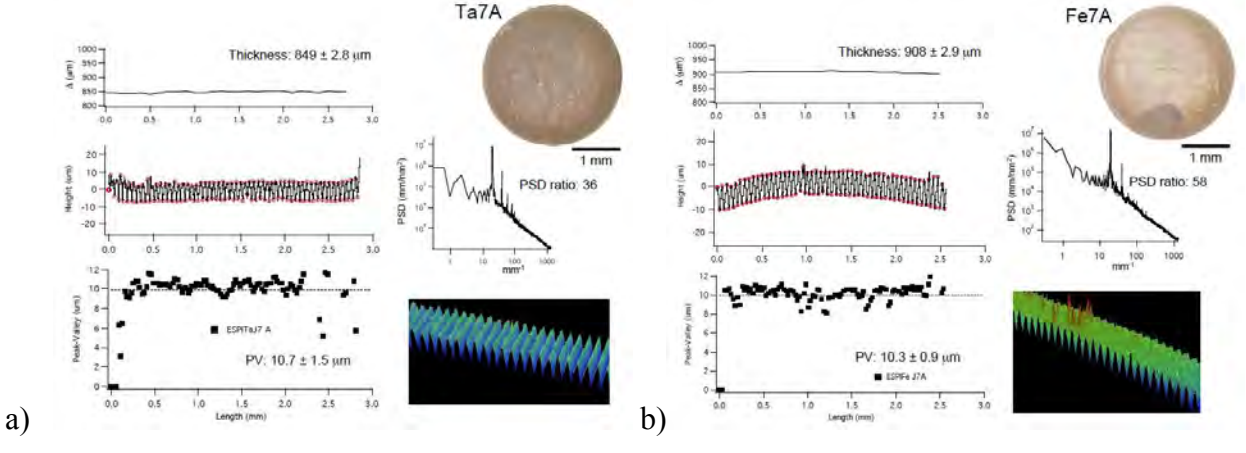

Figure 4: Coining characterization of a laser cut "A" quality a) tantalum target (Ta7A) and b) iron target (Fe7A). Lineouts are taken perpendicular to ripples at center of disc.

C. Target assembly

Ta/SS/PMMA Backing and SS Washers parts were purchased by GA and provided to vendor for machining. PMMA Backing material was purchased from Goodfellow (ME307910). The Ta backing and washer material was also purchased from Goodfellow (TA0079440/24). The Stainless steel backing and washer material was purchased from McMaster Carr (1274T19). The Polystyrene heat shield material was purchased from Goodfellow (ST311250/3).

Heat Shield Materials:

The CHBr material was provided by LLNL and laser machined to the desired shape at GA. There were no issues with the laser machining this material to size.

CHBr material was provided by LLNL and was quoted of having a thickness of 55 μm. The CHBr material was a circular film ~25 mm in diameter. We measured the center of the film using a micrometer to verify the thickness. The micrometer measurement gave a value of 50 μm ± 2. This material was used for both the Janus 12A and 12B experiments. The CHBr HeatShield was cut for the Janus 12A experiments and each part was each individually measured to be 50 μm ± 2.

The 12B Measurement/Data sheet erroneously states that each part was measured. In fact, given the consistency observed in the thickness of the 12A parts, the reported value from LLNL, and the short amount of time (as well as effort available) to prepare the 12B targets, a value of 50 μm was used as a "Batch Measurement" for 12B targets

The left over film from this material was returned to Brian Maddox when it was realized that CHBr would be needed for the Drive Targets. Brian confirmed that this was the material that was given to Schafer for their use.

As a sanity check, since we do not have the measurement on all the 12B parts, we can use the glue gaps to infer an average value for the thickness of the CHBr. The glue gaps to consider are:

PMMA to backing Ta or Fe
PMMA+backing to SS washer
Coined Sample to CHBr HeatShield

The average of all the glue gaps is ~11 microns.

If the CHBr HeatShield was 30 micron for the 12B Strength targets, the glue gap for the Coined Sample to CHBr HeatShield would need to be ~30 micron in thickness. This is inconsistent with all other glue gaps produced in the same timeframe as well as for the 12A Strength Targets. This along with the consistency seen in the thickness of the CHBr HeatShield for the 12A series gives reasonable confidence in the thicknesses reported for the 12B strength targets.

We further received the left over CHBr material from Schafer. This was re-measured to be ~48-50 μm, the thinnest being 44 μm.

The 250 μm CH material was obtained from Goodfellow and it had a large variation of +/-20%. Consequently, the film was mapped for thickness to provide an area that satisfied the desired thickness.

Assembly:

Target assembly was straight forward with no issues. Two types of adhesives used were used to make these targets. For adhesives that allowed us to glue transparent material such as the PMMA backing and CHBr Heat shield, Norland 61 (UV epoxy glue) from Norland Products (NOA-61) was used and cured using UV point light source (Panasonic UV curing system Model ANUJ5014V2) for 2-3 minutes. For parts that were not transparent such as the rippled foils, SS and Ta washers, and the Al coated PS heat shield, a, 3-minute epoxy glue was used from Hardman (04001). Both adhesive types were applied via a small applicator tip. The glue gaps were measured by measuring the assembled part for it's thickness and the thickness of each part before assembly, and then calculating the glue gap by subtracting the thickness of each part from the total assembled thickness. The glue gaps measured for each part was the gap between the rippled target and the backing material, and the glue gaps between the heat shield and the rippled target. The average glue gap for was measured to be ~11 μm.

III. CONCLUSIONS AND RECOMMENDATIONS

In this work, we polished, coined, and laser cut ~3 mm diameter, ~1 mm thick Ta and Fe discs for JANUS 12B. We diamond turned a 10 μm PV, 50 μm wavelength pattern and found minor discrepancies that indicated clearance issues. Nevertheless, the pattern was acceptable and we used 5 dies for coining. In contrast to thinner 50-500 μm foils that require 2-3 times larger coining stress than the material's yield stress, we found that the required coining stress to pattern a 10 μm peak-to-valley, 50 μm wavelength ripple in these 1 mm thickness discs was approximately equivalent to the bulk yield stress. Furthermore, we found that the discs compress 10-15% during coining and that the degree of compression increases with die age. We hypothesize that the generally lower ripple quality uniformity compared to thin foils is linked to this large compression and specifically the alignment of the die and disc before pressing begins.

Future research should focus on obtaining more uniform patterns and reproducible coining results on these thick discs. Some possibilities to accomplish this include: 1) using a disc that is noticeably larger in area than the die surface 2) using a new die for each coin 3) machining a convex rounded face into the die so that it is less likely to bowl 4) experimenting with a softer flat to take up some of the compression from the disc.

Should deeper patterns be required with this same wavelength, the primary technical difficulty will be the clearance of the diamond turning tool. The clearance was marginal for this work. Deeper patterns could be achieved if the ripple wavelength is increased so as to maintain a similar slope between each peak and valley. Given that the slope of a sine wave ~ PV/λ, if the peak-to-valley is doubled, the wavelength would also need to be doubled. Note that there are custom-made diamond designed tools to increase the clearance. However, they are more expensive, weaker, and untested on nitrided steel.

REFERENCES

(1) G. C. Randall, J. Vecchio, J. Knipping, D. Wall, T. Remington, P. Fitzsimmons, M. Vu, E. Giraldez, B. Blue, M. Farrell, et al., J. Fus. Sci. Tech. accepted for publication (2012).
(2) D. Tabor, The Hardness of Metals (Oxford University Press: Oxford, 1951).
(3) R. Kapoor and S. Nemat-Nasser, Metallurgical and Materials Transactions A 31A, 815 (2000).
(4) V. A. Borisenko, V. K. Kharchenko, and V. N. Skuratovskii, Strength of Materials 1, 283 (1969).
(5) H. Conrad and W. Hayes, Trans. ASM 56, 125 (1963).
(6) Y.-G. Jung and B. R. Lawn, J. Mater. Res. 19, 3076 (2004).